Chemical Science

Accepted Manuscript

Volume 1 | Number 1 | Jan 2013 | Pages 1–100

Chemical Science

www.rsc.org/chemicalscience

ROYAL SOCIETY
OF CHEMISTRY

This is an *Accepted Manuscript*, which has been through the Royal Society of Chemistry peer review process and has been accepted for publication.

Accepted Manuscripts are published online shortly after acceptance, before technical editing, formatting and proof reading. Using this free service, authors can make their results available to the community, in citable form, before we publish the edited article. We will replace this *Accepted Manuscript* with the edited and formatted *Advance Article* as soon as it is available.

You can find more information about *Accepted Manuscripts* in the **Information for Authors**.

Please note that technical editing may introduce minor changes to the text and/or graphics, which may alter content. The journal's standard **Terms & Conditions** and the **Ethical guidelines** still apply. In no event shall the Royal Society of Chemistry be held responsible for any errors or omissions in this *Accepted Manuscript* or any consequences arising from the use of any information it contains.

ROYAL SOCIETY
OF CHEMISTRY

www.rsc.org/chemicalscience

Chemical Science

RSCPublishing

ARTICLE

Stable luminescent iridium(III) complexes with bis(N-heterocyclic carbene) ligands: photo-stability, excited state properties, visible-light-driven radical cyclization and CO2 reduction, and cellular imaging†

Chen Yang,[ab] Faisal Mehmood,[a] Tse-Lung Lam,[c] Sharon Lai-Fung Chan*[c], Yuan Wu,[a] Chi-Shun Yeung,[a] Xiangguo Guan,[a] Kai Li,[ab] Clive Yik-Sham Chung,[a] Cong-Ying Zhou,[ab] Taotao Zou,[a] and Chi-Ming Che*[ab]

A new class of cyclometalated Ir(III) complexes supported by various bidentate C-deprotonated (C^N) and *cis*-chelating bis(N-heterocyclic carbene) (bis-NHC) ligands has been synthesized. These complexes display strong emission in deaerated solutions at room temperature with photoluminescence quantum yields up to 89% and emission lifetimes up to 96 µs. A photo-stable complex containing C-deprotonated fluorenyl-substituted C^N shows no significant decomposition even upon irradiation for over 120 h by blue LEDs (12 w). These, together with the strong absorptions in the visible region and rich photoredox properties, allow the bis-NHC Ir(III) complexes to act as good photo-catalysts for reductive C−C bond formation from $C(sp^3/sp^2)$−Br bonds cleavage using visible-light irradiation ($\lambda > 440$ nm). A water-soluble complex, with glucose-functionalized bis-NHC ligand, catalyzed visible-light-driven radical cyclization for synthesis of pyrrolidine in aqueous media. Also, the bis-NHC Ir(III) complex in combination with cobalt catalyst can catalyze visible-light-driven CO_2 reduction, with excellent turnover number (> 2400) as well as selectivity (CO over H_2 in gas phase: $> 95\%$) can be achieved. Additionally, this series of bis-NHC Ir(III) complexes are found to localize in and stain endoplasmic reticulum (ER) of various cell lines with high selectivity, and exhibit high cytotoxicity towards cancer cells, revealing their potential uses as bioimaging and/or anti-cancer agents.

Introduction

Luminescent organometallic complexes of 3rd row transition metals, such as Ir,[1-5] Pt,[6-11] Au[12-19] are currently receiving burgeoning interest due to their profound applications in materials science,[20-22] biology,[23, 24] organic synthesis.[25-27] In particular, the favourable emission properties of cyclometalated Ir(III) complexes have been harnessed for applications by many research groups with examples such as the development of high performance OLEDs by Thompson and co-workers [3-5, 28-31] and the design of bioimaging and cellular probes by Lo and co-workers.[32-36] Over the past decade, as a result of the extensive works most notably by MacMillan,[37, 38] Yoon,[27, 39-41] and Stephenson and co-workers, [42-45] luminescent cyclometalated iridium(III) complexes are widely used in photo-redox catalysts, which has been shown to have useful applications in organic synthesis.

In 2008, Yoon and co-workers[40] reported [2+2] enone cycloadditions, as well as MacMillan and co-workers[38] published alkylation of aldehydes, both of which were catalyzed by triplet metal-to-ligand-charge-transfer (^{3}MLCT) excited state of $[Ru(bpy)_3]^{2+}$ generated upon visible-light irradiation. Subsequently, Stephenson and co-workers unfolded reductive dehalogenation of activated alkyl halides catalysed by $[Ru(bpy)_3]^{2+}$,[44] and reductive dehalogenation of alkyl, alkenyl and arly iodides by using *fac*-Ir(ppy)$_3$[45] as photo-redox catalyst. Compared to $[Ru(bpy)_3]^{2+}$ and *fac*-Ir(ppy)$_3$, the application of luminescent platinum(II) on photocatalysis is still nascent. Recently, our group and Wu's group demonstrated that pincer Pt(II) complexes are capable of catalysing light induced C-C bond formation.[46, 47]

The important features that endow luminescent transition metal complexes to act as useful photo-redox catalysts or photo-sensitizers for light induced reactions include: 1) the long lifetime of their electronic states, thus allowing bimolecular reaction to proceed in solutions, 2) their electronic excited states are both a strong reducing and oxidizing reagent with reduction potentials systematically varied by the auxiliary ligands.[41] For the photo-catalysis to have practical interests, the design of new

Chemical Science

View Article Online

Page 2 of 14

DOI: 10.1039/C5SC04458H

Chemical Science

ARTICLE

highly stable photo-redox catalysts having very long-lived electronic excited states in solution is desirable.
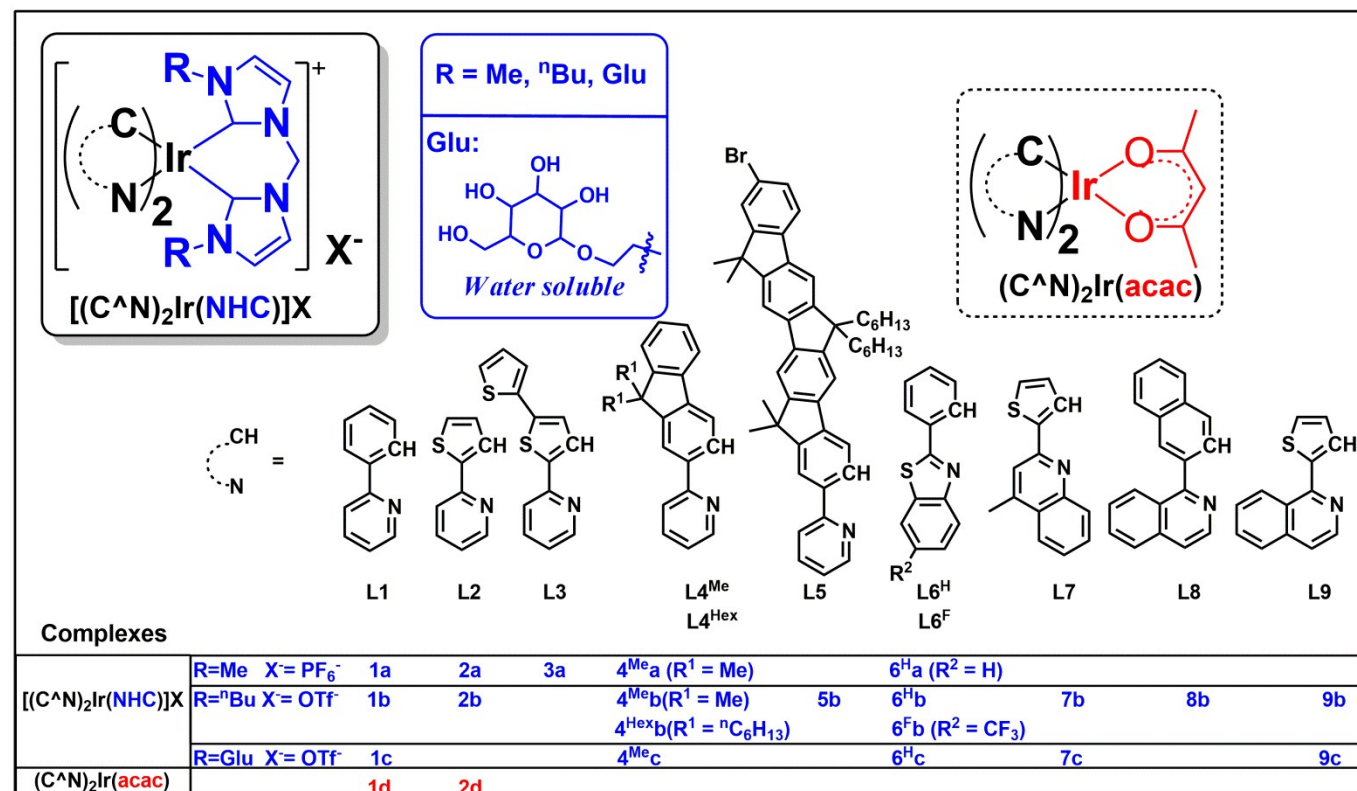

Chart 1. Iridium(III) complexes in this work. Complexes **1a**,[73,74] **1b**,[73] **1d**[28] and **2d**[31] have been reported in literature.

Our endeavour to develop transition metal photo-catalysis is to use visible light for activation of small molecules such as CO_2 described in this work and for C-X bond functionalization. A major consideration is to ultilize the visible-light, which falls within the solar spectrum and avoids deterious high-energy UV-initialized photochemical side reaction(s).[48, 49] In literature, platinum group metal complexes and semi-conductors are usually used as a photo-redox catalyst for photochemical reduction of CO_2.[50] Earlier examples of transition metal photo-catalyst used for photochemical reduction of CO_2 include cobalt porphyrins,[51] Re(bpy)(CO)$_3$Cl[52, 53] and Ir(terpy)(ppy)Cl.[54] More recently, system comprising of *fac*-Ir(ppy)$_3$ in conjunction with [Ni(Prbimiq1)]$^{2+}$,[55] Fe(porphrin),[56] [Co(TPA)Cl]Cl,[57] (TPA = tris(2-pyridylmethyl)amine) and [Co(N5)]$^{2+}$ (N5 = 2,13-dimethyl-3,6,9,12,18-pentaazabicyclo-[12.3.1]octadeca-1(18),2,12,14,16-pentaene)[58] were reported for photochemical reduction of CO_2.

The stability of photo-catalysts is an important issue for practical application of transition metal photochemistry. Numerous studies revealed that the photochemically active excited states of [Ru(bpy)$_3$]$^{2+}$,[59-61] [Ir(ppy)$_2$(bpy)]$^+$,[60, 62] and *fac*-Ir(ppy)$_3$[55, 57, 63] are not stable under light irradiation for a long period of time as a result of dissociation of coordinated ligand(s) presumably via low lying d-d excited state(s). To address the photo-stability issue, we are attracted to the use of N-heterocyclic carbene (NHC) ligands which have been receiving burgeoning attention in coordination chemistry due to their strong σ-donor strength to develop robust metal photo-sensitizer and photo-catalysts.[64-70] Also, the N-substituent of NHC ligands can be used to tune both the physical and chemical properties of

the resultant photo-active transition metal complexes such as their solubility in various solvents including water. NHC ligands functionalized with carboxylate, sulfonate, amine/ammonium, alcohol motif have been reported for the development of water-soluble transition metal catalysts for Suzuki coupling, hydrosilylation, hydrogenation, olefin metathesis and CO_2 reduction.[65, 71]

Compared with Ir(III) complexes supported by the bidentate acetylacetonate[28] and/or 2,2'-bypyridine[1] ligands, the photophysical and application studies of the related bis-NHC Ir(III) complexes are relatively scarce. In 2010, cationic bis-NHC Ir(III) complexes were reported by De Cola and co-workers[72] to have application in blue-light emitting electrochemical cells; subsequently, a number of bis-NHC Ir(III) complexes were reported for photophysical and biological studies.[65, 67, 72-74] In this work, a series of strongly luminescent Ir(III) complexes (Chart 1) containing bis-NHC ligands and visible light absorbing C-deprotonated (C^N) ligands was synthesized and their photophysical and electrochemical properties were examined. These complexes display high photo-stability and are strongly emissive with long lifetimes of up to 96 μs in solutions at room temperature. The water-soluble luminescent Ir(III) complexes, containing the glucose-functionalized NHC ligand, were found to be active photo-catalysts for radical cyclization leading to the formation of 5-membered ring pyrrole in aqueous media with high substrate conversions and yields. One of the photo-stable Ir(III) complexes was utilized as a photo-sensitizer and in conjuction with a recently reported catalyst [Co(TPA)Cl]Cl to convert CO_2 into CO with a turnover number (TON) > 2400, selectivity in gases

phase > 95% and yield of 5.6% (1 mL out of 18 mL of CO_2 was converting into CO at 5 µM concentration of Co complex). Some of the complexes were also demonstrated as potential bioimaging and/or anti-cancer agents.

Results

Synthesis, characterization and photo-stability of [(C^N)₂Ir(NHC)]X complexes

The structures of 18 bis-NHC Ir(III) complexes synthesized in this work (**1c** and **2a**, **2b**, **3–9**), together with previously reported Ir(III) complexes **1a**,[73,74] **1b**,[73] **1d**[28] and **2d**[31], are depicted in Chart 1. Complexes **1–9** were synthesized in good yields by refluxing [(C^N)₂Ir(µ-Cl)]₂ with bis(imidazolium) salts in the presence of silver(I) oxide in 2-methoxyethanol. Details of synthesis and characterization data of ligands and complexes are provided in the ESI†. Notably, ¹H NMR spectra of **7b** and **7c** show poorly resolved peaks in the aromatic region (6.7–8.2 ppm) at ambient temperture, and hence ¹H NMR spectra are recorded from 238 K to 300 K (Fig. S1, ESI†) in order to assure the purity of **7b** and **7c**.

Complexes **1a–4Mea**, **1b–4Meb**, **4Hexb–9b** with *N*-methyl or *N*-butyl substituent on bis-NHC ligands are soluble in most common aprotic solvents, but not in protic solvents e.g. methanol (MeOH) or water. Complexes **1c**, **4Mec**, **6Hc**, **7c** and **9c** with glucose functionalized bis-NHC ligand are soluble in MeOH, ethanol (EtOH) and water.

The photostability of these Ir(III) complexes with bis-NHC ligands was examined by using **4Meb** and **6Hb** as representative examples. **4Meb** and **6Hb** in degassed deuterated MeCN were irradiated using blue light (12 w blue LEDs) for 5 days. The

photolysis, if any, was monitored by ¹H NMR spectroscopy. As depicted in Fig. 1a, in the case of **4Meb**, less than 5% of the complex was observed to undergo photochemical decomposition even after irradiation of 120 h, revealing its outstanding photo-stability. Under the same conditions, Ru(bpy)₃Cl₂, *fac*-Ir(ppy)₃ and [(dFCF₃ppy)₂Ir(dtbbpy)]PF₆ (dFCF₃ppy = 3,5-difluoro-2-[5-(trifluoromethyl)-2-pyridinyl]phenyl; dtbbpy = 4,4'-bis(1,1-dimethylethyl)-2,2'-bipyridine)) were found to decompose after 10 h irradiation as revealed by the changes of their ¹H NMR spectra (Fig. 1c).

Interestingly, irradiation of **6Hb** using blue LEDs for 10 h led to a clean and quantitative conversion to a new species which did not show further changes upon subsequent irradiation for another 90 h (Fig. 1b, this species is noted as **cis-6Hb**). The yield of scale synthesis of **cis-6Hb** from the irradiation of degassed MeCN solution of **6Hb** (100mg in 4 mL MeCN) was 94%. **cis-6Hb** was found to be stable upon standing in solution under dark for another 40 h, or exposed to air for another 20 h (Fig. S2, ESI†). To verify that the transformation of **6Hb** to **cis-6Hb** was caused by visible-light irradiation, a negative control experiment was conducted by keeping **6Hb** in deuterated MeCN in dark (Fig. S2, ESI†), and no structural changes was detected by ¹H NMR spectroscopy.

UV-vis absorption, emission and excitation spectra of **cis-6Hb** measured in DCM solution at 298 K are different from those of **6Hb** with hypersochromic shifts in peak maxima (Fig. 1e). The emission band for **cis-6Hb** displays vibronic spacings of 1245 cm⁻¹ while that of **6Hb** shows spacings of 908 cm⁻¹. Taken into consideration of ESI-MS and spectroscopic data of **cis-6Hb**, **cis-6Hb** is likely a structural isomer for **6Hb**. The exact structure of **cis-6Hb** has been determined by X-ray crystallography.
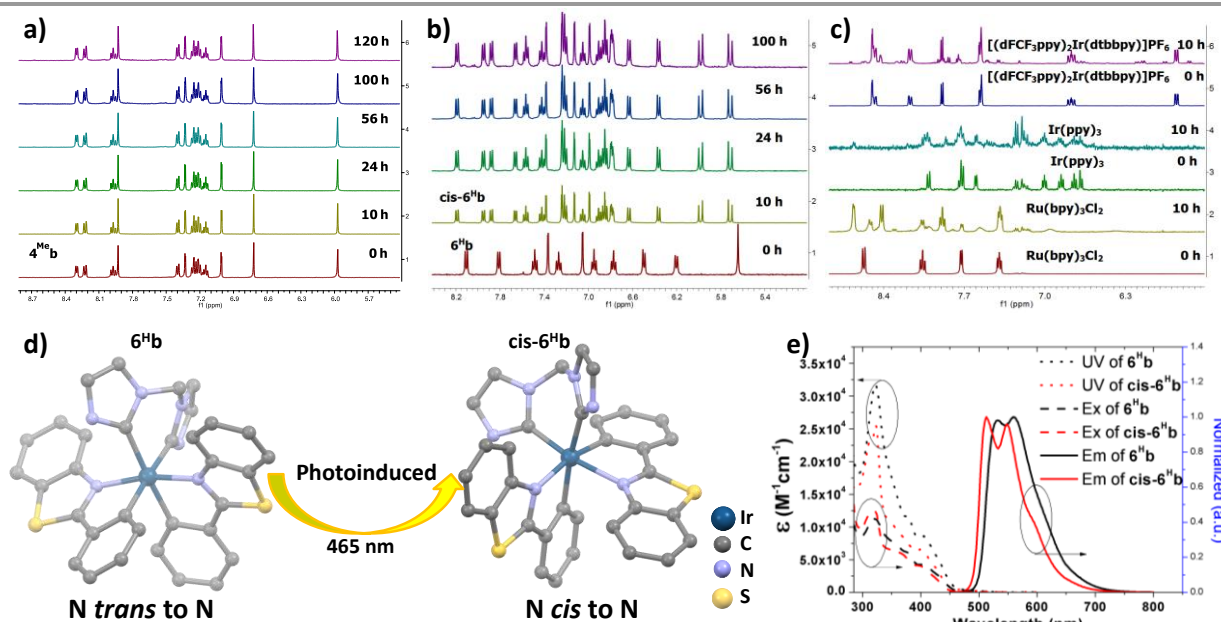

Fig. 1. ¹H NMR spectra for a) **4Meb**; b) **6Hb**; c) Ru(bpy)₃Cl₂, *fac*-Ir(ppy)₃ and [(dFCF₃ppy)₂Ir(dtbbpy)]PF₆ in deuterated MeCN solution for irradiating by blue light (12 W, λ_{max} = 462 nm)[46] (all solutions are degased by nitrogen gas for 10 min); d) crystal structure diagrams showing the photoinduced transformation of coordination for Ir metals in **6Hb** and **cis-6Hb** (butyl group on bis-NHC ligand and hydrogen atoms are omitted for clarity); e) UV/Vis absorption (dotted line), excitation (dashed line) and emission (solid line) spectra of solutions of **6Hb** and **cis-6Hb** (concentration of 2.0 × 10⁻⁵ M) in degassed DCM at 298 K.

X-ray crystallography

Crystals of **4Meb** (with PF₆⁻ counter anion), **6Hb**, **cis-6Hb** and **7b** suitable for X-ray crystallographic analysis were obtained by

slow diffusion of diethyl ether into DCM (**6Hb**), MeCN (**4Meb** and **7b**) and chloroform (**cis-6Hb**) solution of these complexes, respectively. Perspective views of **6Hb** and **cis-6Hb** are shown in Fig. 1d (those of **4Meb**, **7b** are shown Fig. S3 in ESI†). Selected

ARTICLE

bond lengths and angles are compiled in Table S1 (ESI†). Similar to the reported examples,[72] **6^{H}b** adopts a distorted octahedral geometry (Fig. 1), the iridium atom is coordinated by two cyclometalated C^N ligands and one bis-NHC ligand. The two C^N ligands adopt a mutually eclipsed configuration, with the two N atoms (N1 and N2) *trans* to each other and with Ir-N bond length of 2.067(2) and 2.071(2) Å. The two substituted phenyl rings are oriented *cis* to each other with Ir-C bond length of 2.054(2) and 2.077(2) Å. The C^{NHC} atoms of bis-NHC ligand are *trans* to two C atoms from C^N ligands. The Ir-C^{NHC} distances of 2.105(2) Å and 2.128(2) Å are comparable to the

literature values of Ir-C^{NHC} bonds *trans* to phenyl groups.[72] The C^{NHC}-Ir-C^{NHC} bite angles of **4^{Me}b** (84.7(3) º), **6^{H}b** (85.10(9)º), **7b** (85.58(6)º) and that of reported [(dfppy)$_2$Ir(NHC^{Me})]PF$_6$ (85.28(15)º) (dfppy = 4,6-difluoro-phenylpyridine) are consistent.[72] The structures of **4^{Me}b** and **7b** are in line with that of **6^{H}b**. Interestingly, for **cis-6^{H}b** the N atoms from the two C^N ligand are *cis* to each other (Fig. 1d), indicating that **6^{H}b** and **cis-6^{H}b** are structural isomers. The crystallographic refinement parameters for **4^{Me}b**, **6^{H}b**, **cis-6^{H}b** and **7b** are summarized in Table S2 (ESI†).

Table 1. Photophysical data of complexes **1–9**.

Complex	Medium^a	Absorption λ_{max}/nm ($10^{-3}\varepsilon$/M^{-1}cm^{-1})	Emission λ_{em}/nm (τ/µs)	Φ/%^{d}
1a	CH$_2$Cl$_2$	255 (26.8), 267 (24.9), 311 (10.6), 342 (6.1), 380 (3.7), 416 (1.2)	470 (2.1), 499, 534	89
1b	CH$_2$Cl$_2$	254 (36.8), 266 (35.5), 311 (15.5), 342 (9.1), 381 (5.82), 416 (2.16)	470 (2.1), 500, 534	89
1c	H$_2$O	254 (36.8), 266 (35.5), 311 (15.5), 342 (9.1), 381 (5.82), 416 (2.16)	469 (2.0), 498, 534	89
2a	CH$_2$Cl$_2$	252 (13.5), 290 (21.7), 332 (12.6), 369 (6.07), 405 (4.92)	530, 547, 570 (3.03)	11.1
3a	CH$_2$Cl$_2$	252 (15.5), 282 (15.1), 313 (20.5), 335 (23.1), 375 (21.9), 389 (20.9), 440 (20.9)	472, 674 (4.8), 824	0.2
4^{Me}a	CH$_2$Cl$_2$^{b}	260(31.4), 297 (30.0), 316 (33.5), 334 (32.3), 360 (22.4), 378 (16.8), 421 (10.5)	524, 564 (28.6), 614	65
4^{Me}b	CH$_2$Cl$_2$^{b}	267(52.2), 297 (46.8), 316 (50.9), 335 (49.0), 358 (36.3), 376 (27.3), 421 (16.2)	525, 566 (28.7), 614	75
4^{Hex}b	CH$_2$Cl$_2$^{b}	268(42.1), 299 (42.3), 320 (50.4), 338 (49.2), 364 (32.6), 379 (25.6), 421 (14.6)	527, 568 (32.7), 616	82
5b	CH$_2$Cl$_2$^{c}	260 (54.1), 273 (42.5), 310 (32.9), 323 (34.8), 377 (67.2), 398 (97.0), 436 (71.6)	576 (96.1), 625, 683	22.6
6^{H}b	CH$_2$Cl$_2$	271 (23.0), 321 (25.0), 377 (9.57), 407 (6.81), 436 (3.38)	531, 560(6.4)	78
6^{H}c	H$_2$O	268 (21.4), 321 (22.1), 377 (8.06), 407 (5.49), 436 (2.42)	536, 560 (5.0)	66
6^{F}b	CH$_2$Cl$_2$	270 (23.0), 323 (32.1), 383 (10.7), 415 (7.88), 447 (4.08)	530, 558(3.2)	68
7b	CH$_2$Cl$_2$	296 (26.8), 333 (18.5), 388 (9.31), 437 (7.76), 467 (4.60)	582, 623 (6.2)	36
7c	H$_2$O	293 (25.9), 330 (17.4), 386 (9.63), 432 (6.92), 464 (3.71)	583, 622 (5.9)	32
8b	CH$_2$Cl$_2$	260 (80.1), 290 (48.5), 315 (35.4), 376 (34.5), 429 (7.52), 485 (3.47), 494 (2.88)	618, 659(5.2)	3
9b	CH$_2$Cl$_2$	313 (24.2), 334 (23.8), 384 (12.7), 428 (10.7), 457 (8.20), 485 (3.47)	617, 667(7.4)	13
9c	H$_2$O	315 (18.4), 380 (9.69), 420 (7.6), 454 (4.95), 475 (2.15)	620 (4.5), 668	9

^{a} Measured in degassed CH$_2$Cl$_2$ and water (2.0×10^{-5} M) at 298 K. ^{b} **4^{Me}a**, **4^{Me}b** and **4^{Hex}b** were measured at the concentration of 5×10^{-6} M. ^{c} **5b** was measured at the concentration of 1×10^{-6} M. ^{d} Phosphorescence quantum yields were measured by using [Ru(bpy)$_3$](PF$_6$)$_2$ (Φ = 0.062 in MeCN) as standard.

Electronic absorption and emission spectroscopy

Photophysical data of **1−9** including their UV/Vis absorption and emission maxima, emission lifetimes and photo-luminescent quantum yields are tabulated in Table 1. All the complexes show intense high-energy absorptions ranging from 250 to 380 nm and lower-energy absorptions at 416 − 494 nm (Fig.2, 3 and S4 in ESI†). The high-energy absorptions are attributed to the $^1\pi\rightarrow\pi^*$ transition of the ligands, whereas the low energy absorption bands should be ascribed to the admixture of metal-to-ligand charge transfer (MLCT) transitions and ligand-ligand charge transfer (LLCT) transitions.[72] The charge transfer (CT) assignment is further supported by the energy trend observed in the complexes with different C^N ligands. For example, the low-energy absorptions of **8b** and **5b** reveal significant red-shifts from those of **1b** and **4^{Me}b** respectively. This can be rationalized by the extended π-conjugation of the C^N ligand in **8b** and **5b**, leading to the lowering of the π*(C^N) orbitals and hence decreases in CT energy. These red-shifts in the UV-vis absorptions, together with the large molar absorptivities in the visible region (e.g., **5b**: 7.2×10^4 M^{-1}cm^{-1}), allow the complexes to show strong absorptions in the visible region. This is believed to be crucial for harvesting visible-light in solar-spectrum as well as avoiding UV-initiated side reactions due to the use of UV in the photo-catalysis by the Ir(III) complexes. As revealed by the UV absorption spectra of **6^{F}b** and **6^{H}b** (Fig. S4b, ESI†), a bathochromic shift about 500 cm^{-1} are observed for the lower-energy absorption band(s). These could be attributed to the

electron-withdrawing group of CF$_3$ on the cyclometalated ligand which lowers the C^N based LUMO level.
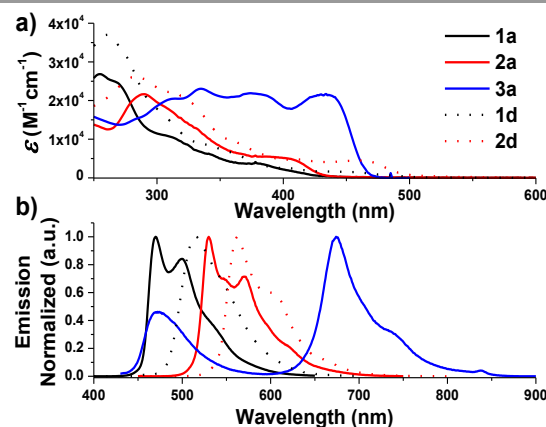

Fig. 2. UV-Vis absorption (top) and emission (bottom) spectra of solutions of **1a − 3a** and **1d − 2d** in degassed DCM (concentration of 2.0×10^{-5} M) at 298 K.

On the other hand, the *N*-alkyl substituents on bis-NHC ligand are found to have only minor effect, if any, on the UV/Vis absorption spectra of the Ir(III) complexes, as revealed by the overlaid spectra of the group of **1a**, **1b**, **1c** (Fig. S4a, ESI†). Complex **1a** absorb weakly at the wavelength from 430 nm to 500 nm with molar absorptivity less than 500 M^{-1}cm^{-1} in contrast to the high values of 2500 M^{-1}cm^{-1} for **1d** having same C^N

Page 5 of 14

Chemical Science

View Article Online
DOI: 10.1039/C5SC04458H

Chemical Science

ARTICLE

luminophore, respectively. The calculated wavelength for ground stated HOMO→LUMO (S_0→S_1 transition) is 369 nm and 414 nm for **1a** and **1d**, respectively (Fig. S4e–S4f, ESI†). These calculated values are in reasonable agreement with the corresponding experimental absorption λ_{max} values 410 and 460 nm respectively.
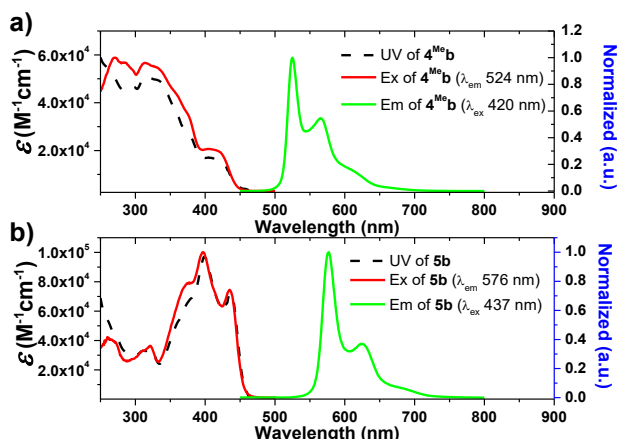

Fig. 3 UV/Vis absorption (black dashed line), excitation (red solid line) and emission (green solid line) spectra of solutions of a) **4^{Me}b** (5.0×10^{-6} M); b) **5b** (1.0 ×10^{-6} M) in degassed DCM at 298 K.

Complexes **1**–**9** display strong phosphorescence in deaerated solution at room temperature. (Fig. 2, 3 and S4 (ESI†); Table 1) All the complexes show vibronic-structured emissions, and their emission lifetimes are found to be in microsecond regime. For example, **4^{Me}b** exhibits structured emission bands with vibrational spacings of ~ 1380 cm^{-1} and long emission lifetime of 28.2 μs. Only small negative solvatochromic effect on the emission at 524 nm is found (± 5 nm; Fig. S4d, ESI†). These findings, together with TD-DFT calculations, suggest that the photoluminescence of the complexes is derived from triplet metal-perturbed ligand-centred (^{3}LC) π–π* excited states. On the other hand, the structureless emission of **1d** (the acetylacetonate (acac) analogous of **1a**) at 516 nm should be ascribed to the ^{3}MLCT/LLCT emission.[2] Interestingly, complex **3a** (Φ = 0.2%; τ = 4.8 μs) displays dual emission (Fig. 2) in contrast to the single emission of the acac analogous **3d**,[75] suggesting the possibility of modulation of photophysical properties of Ir(III) complexes by the NHC ligands.

Changes in chemical structure of the cyclometalated ligands also result in profound effect on the photophysical properties of the Ir(III) complexes. For example, **5b** displays a significant red-shift in emission maximum (576 nm) when compared to that of **4^{Me}b** and **4^{Hex}b** (525 and 527 nm respectively). This can be rationalized by the extended π-conjugation of the C^N ligands, leading to the decrease in energies of metal-perturbed ^{3}LC emission. Moreover, for **4^{Me}a**, **4^{Me}b** and **4^{Hex}b**, their photoluminescence quantum yields in solutions are affected by the substituents on fluorenyl moiety as well as the N-alkyl groups of the bis-NHC ligands, e.g. complex **4^{Hex}b** exhibits higher photoluminescence quantum yield than **4^{Me}a** and **4^{Me}b**. This is probably attributed to the fact that the long hexyl and N-butyl chains disfavour intermolecular stacking interactions among the planar C^N ligands, leading to reduced triplet-triplet annihilation and a higher photoluminescence quantum yield can be achieved.

In addition, **5b** shows a significantly longer emission lifetime (96.1 μs) than **4^{Me}b** (28.7 μs). This might be owing to the reduced metal character in the electronic excited state of **5b**, and hence slower triplet radiative decay. Similarly, with a smaller parentage of metal character in the frontier molecular orbitals, **6^{H}b** (6.4 μs) shows a longer emission lifetime than **6^{F}b** (3.2 μs). These long-lived triplet excited states allow the Ir(III) NHC complexes to undergo a variety of photochemical reactions, notably for visible-light-driven photo-catalytic reductive C–Br bond cleavage and CO_2 reduction which will be illustrated later.

Electrochemistry

Table 2. Electrochemical data^a of bis-NHC Ir(III) complexes.

Complex	$E_{pa}{}^b$/V	$E_{pc}{}^c$/V
1b	0.87	-2.52
2a	0.64	-2.24
4^{Me}a	0.74	-2.41
4^{Me}b	0.79	-2.40
4^{Hex}b	0.74	-2.44
5b	0.72	-2.25
6^{H}b	0.98	-2.14
6^{F}b	1.04	-1.94
7b	0.69	-2.09
8b	0.62	-1.94
9b	0.62	-2.16

^{a} Supporting electrolyte: 0.1 M ^{n}Bu$_4$NPF$_6$ in MeCN and values are recorded vs Ag/AgNO$_3$ (0.1 M) in MeCN; Cp$_2$Fe$^{+/0}$ occurs at the range of 0.05–0.08 (V) vs Ag/AgNO$_3$. ^{b} Values refer to oxidation peak potential (E_{pa}) at 25 °C for irreversible couples at a scan rate of 100 mV s^{-1}. ^{c} Values refer to reduction peak potential (E_{pc}) for the irreversible reduction waves.

The electrochemical data of **1b** – **9b** are summarized in Table 2 (all values versus Ag/AgNO$_3$, scan rate of 100 mV s^{-1}, 0.1 M ^{n}Bu$_4$NPF$_6$ in MeCN as supporting electrolyte) and Table S3 (values vs Cp$_2$Fe$^{+/0}$, ESI†). These complexes display one irreversible oxidative wave at E_{pa} = 0.62 − 1.04 V and one irreversible reductive wave at E_{pc} = -2.52 − -1.94 V (vs Ag/AgNO$_3$). The cyclic voltammograms of **1a** have been reported elsewhere[74] with the oxidation potential of +1.16 V (vs Ag/AgNO$_3$) in CH$_2$Cl$_2$. By comparing with the electrochemical data of **1d** and **2d**[2] both of which have ancillary acac ligand, the first oxidation wave of **1a** should originate from Ir(III)-centred/C^N ligand-centred oxidation. This assignment is further supported by the observation of more positive oxidation potential of **6^{F}b** (+1.04 V) than that of **6^{H}b** (+0.98 V). The electron-withdrawing −CF$_3$ group of **6^{F}b** will lower the energy levels of d(Ir) and π(C^N) orbitals, leading to the more positive oxidation potential of **6^{F}b**. On the other hand, **4^{Me}b** and **5b** have more extended π-conjugated C^N ligands than **1b**. This will result in an increase in the energy level of π(C^N) and/or d(Ir) orbitals, thus **4^{Me}b** and **5b** can undergo oxidation more readily than **1b** and hence less positive oxidation potential are found.

Compared with **1b**, [(dfppy)$_2$Ir(bis-NHC^{Bu})]PF$_6$[72] displays a more anodic oxidation potential of E_{ox}= 1.04 V and the similar reduction potential of E_{re}= -2.37 V (vs Cp$_2$Fe$^{+/0}$), which is

Chemical Science

View Article Online
DOI: 10.1039/C5SC04458H

Page 6 of 14

ARTICLE

Chemical Science

attributed to stabilization of HOMOs as a result of the presence of highly electron-withdrawing F substitution on C^N ligand (dfppy). For the irreversible reduction wave, a less negative reduction potential is found for $6^H b$ (E_{pc} = -2.14 V vs Ag/AgNO$_3$, Table 2, Fig. S4), as compared to that of $1b$ (E_{pc} = -2.52 V vs Ag/AgNO$_3$, Table 2, Fig. 4) which has a less extended π-conjugation of the C^N ligand. The reductive wave is further anodically shifted in the case of $6^F b$ (E_{pc} = -1.94 V vs Ag/AgNO$_3$, Table 2, Fig. S5a, ESI†). Therefore, the reduction process should be localized on the C^N ligands.
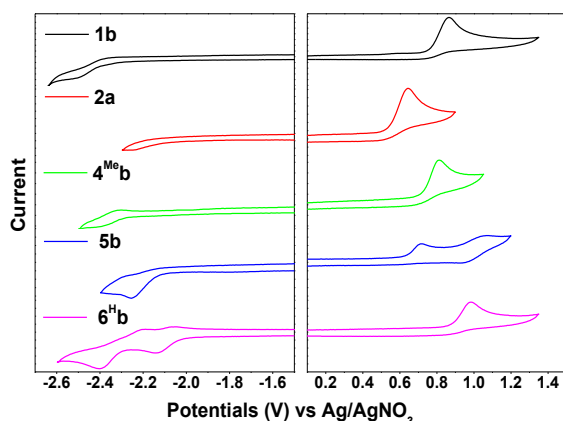

Fig. 4 Cyclic voltammograms of $1b$, $2a$, $4^{Me}b$, $5b$ and $6^H b$ in MeCN with ^{n}Bu$_4$NPF$_6$ (0.1 M) as supporting electrolyte. Conditions: glass-carbon, working electrode, scan rate: 100 mV s^{-1}.
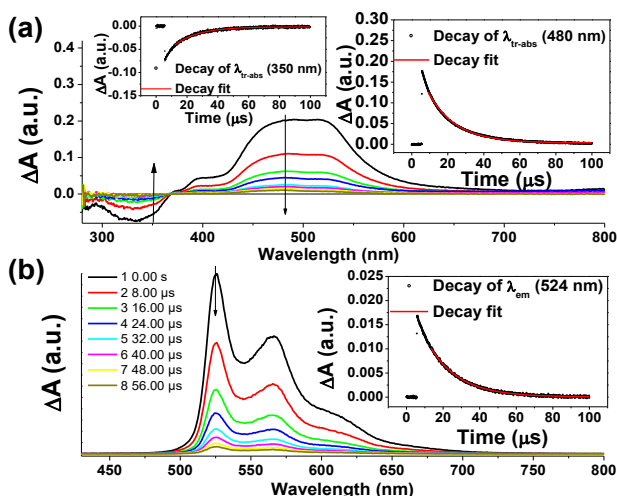
Excited states properties

Fig. 5 Time-resolved spectra of $4^{Me}b$ a) tr-abs (inserts: decay of tr-abs at λ = 350 nm and 480 nm); b) tr-em (decay of tr-em at λ = 524 nm) spectra recorded at specified time after laser pulse excitation (355 nm) in degassed MeCN at 298 K.

Nano-second transient absorption and emission spectroscopic (tr-abs and tr-em) measurements were undertaken for the highly emissive bis-NHC Ir(III) complexes with long-lived electronic excited states i.e. $4^{Me}b$ (Fig. 5) and $4^{Me}c$ (Fig. 6a) in MeCN and water respectively. These two complexes have the same lumophore but different functionalized NHC groups, leading to the distinguishing solubility in solvents, such as one is soluble in

organic solvent and the other in water. The tr-abs and tr-em spectra of the other bis-NHC Ir(III) complexes e.g. $5b$ in MeCN (Fig. S6a, ESI†), and $6^H c$ (Fig. S6b, ESI†) in water were also recorded and the results could be found in ESI†.

The time-resolved absorption and emission spectra of $4^{Me}b$ recorded at various time intervals after excitation at 355 nm are depicted in Fig. 5. Kinetic decay analysis of bleaching of ground-state of $4^{Me}b$ ($\tau_{350\ nm}$ =15.4 μs, Fig. 5a, left insert) matches well with growth of the absorption of triplet excited state ($\tau_{480\ nm}$ = 15.2 μs, Fig. 5a, right insert) as well as the emission lifetime ($\tau_{524\ nm}$ = 16.5 μs, Fig. 5b, right insert) in MeCN at 298 K.
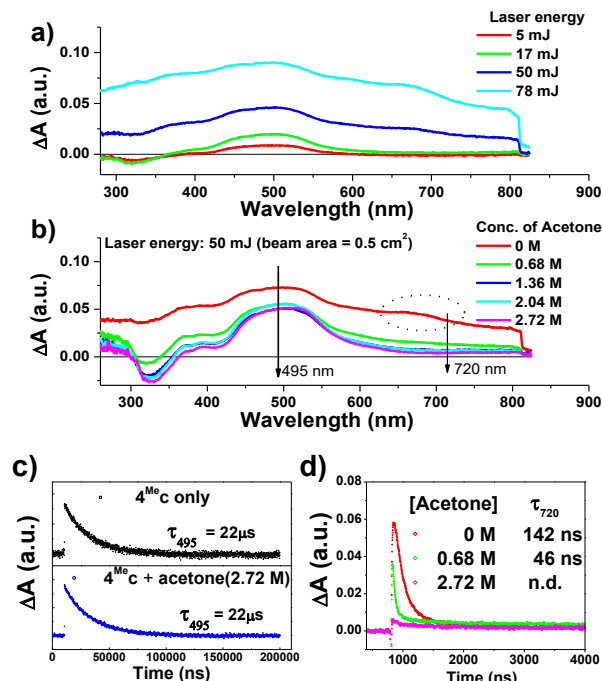

Fig. 6 Transient absorption spectra recorded a) under specified laser energy; b) in presence of specified concentration of acetone of a degassed aqueous solution of $4^{Me}c$ (about 1×10^{-5} M); kinetic studies of c) λ_{tr-abs} (495 nm) and d) λ_{tr-abs} (720 nm) under absence/presence and specified concentrations of acetone.

The transient absorption spectra of $4^{Me}c$ in aqueous solution recorded at different energies of laser beams (355 nm) reveal different spectral changes. As depicted in Fig. 6a, in addition to the growth of the absorption of triplet excited state of $4^{Me}c$ from 380 to 700 nm, an emergence of absorption band from 650 to 730 nm was observed as laser pulse energy ≥ 50 mJ (beam area: 0.5 m^2). This absorption band could be quenched upon addition of acetone (Fig. 6b and Fig. S7a and S7b, ESI†), but no quenching of transient absorption at 594 nm and emission at 524 nm were observed in the presence of acetone (Fig. 6c and S7, ESI†). The decay rate constant monitored at 720 nm of $4^{Me}c$ (Fig. 6d, absence of acetone) was much faster than that measured at 495 nm in Fig. 6c/S7c and decay of emission at 524 nm (Fig. S7d, ESI†). In view of these different kinetic behaviours, the transient absorption from 650 to 730 nm depicted in Fig. 6b might originate from hydrated electrons e_{aq^-},[76, 77] which were formed by the photo-induced ionization of $4^{Me}c$ in aqueous solution upon excitation with high energy laser beams. This is in line with a reported photoionization of [Pt$_2$(POP)$_4$]$^{4-}$,[78] as well as the findings in the studies of solvated electron with acetone.[79, 80] Similarly, complex $6^H c$ in aqueous solution was also observed to undergo photo-ionization as revealed by the increase in transient

absorption in the region of 600 to 700 nm (Fig. S8b, ESI†). For **4^Me b**, its transient absorption spectra monitored at high laser pulse energy in MeCN exhibits similar profile as that of lower energy (Fig. S8b−S8c, ESI†). However, newly generated long-lived species has been observed at high laser pulse energies after 100 μs (Fig. S8b−S8e, ESI†), revealing that photo-ionization of **4^Me b** with the generation of [**4^Me b**]^+ (Ir(IV)) is likely occurred. The accompanying solvated electrons is not observed in this case due to readily quenching by MeCN.[81]

Based on the electrochemical data and the determination of E_{0-0} from the spectroscopic measurements, the photoredox properties of the bis-NHC Ir(III) complexes can be estimated (Table S3, ESI†). The triplet excited states of the complexes are found to be powerful oxidants and reductants, and some of them are even more reactive towards photoredox reactions than [Ru(bpy)$_3$]$^{2+}$ and fac-Ir(ppy)$_3$. A representative example is **4^Me b** (E(Ir$^{IV/III*}$) = -1.51 V vs SCE), which is a stronger reductant than [Ru(bpy)$_3$]$^{2+}$ (E(Ru$^{III/II*}$) of -0.81 vs SCE).[37, 82] As a result, it is anticipated that the bis-NHC Ir(III) complexes described herein, upon photoexcitation in the visible-light region, can catalyse a number of reactions which are not feasible by the widely used [Ru(bpy)$_3$]$^{2+}$.

Previous reports
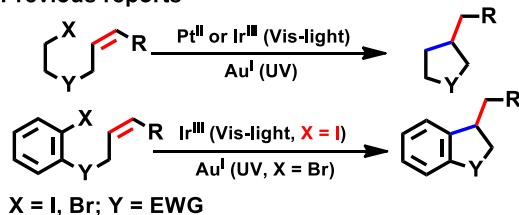
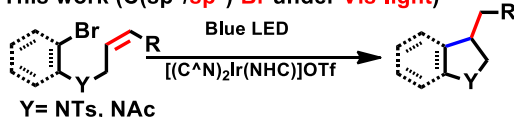**This work (C(sp^3/sp^2)-Br under Vis-light)**

Y= NTs, NAc

Chart 2. General photocatalytic reactions by cyclometalated complexes. EWG = electron-withdrawing group.

Photocatalysis

With good photo-stability, long excited state lifetime, favourable absorption in the spectral region of blue LED and tunable photo-redox properties, these bis-NHC Ir(III) complexes have been investigated for photo-redox reactions (Chart 2), examples of which are described in the following section.

We are attacted to a recent work by Lee and co-workers[83] on visible-light-induced reductive cyclization of aromatic iodides and bromides to form indoline using [(ppy)$_2$Ir(dtbbpy)]PF$_6$ as photo-catalyst (PC). Yet, aryl bromides are found to be less reactive than the iodides.[84] Barriault and co-workers addressed this issue by using dinuclear gold(I) complexes ([Au$_2$(dppm)$_2$]OTf$_2$) as the photo-catalyst.[85] However, this gold complex only shows absorption at high-energy UV region (λ < 300 nm), which may result in destructive effect on the products and/or lead to undesired side reactions.

Table 3. Screening bis-NHC Ir(III) complexes for photo-catalysis.*

Entry[a]	PC	Conversion/%[b]	Yield/%[b]
1	**1b**	93	59
2	**2b**	1	0
3	**4^Me b**	90	59
4	**5b**	90	52
5	**6^H b**	93	59
6	**6^F b**	80	44
7	**7b**	49	24
8	**8b**	11	7.3
9	**9b**	0.1	0

*Complex 3a was not tested because of the low quantum yield (0.2 %, see Table 1). [a] Procedure: Substrate 50 μmol, **PC** (1 mol%), DIPEA (5 equiv.), HCOOH (2.5 equiv.) in 4 mL MeCN solution was degassed by nitrogen, and irradiated by blue light (12 W, λ_{max} = 462 nm) at ambient temperature for 4 h. [b] Determined by ^{1}H NMR spectroscopy by adding internal standard of 5,5'-dimethyl-2,2'-bipyridine.*

Table 4. Visible-light-induced C-C bond formation for aryl halide.

Entry[a]	PC (Substrate)	Amines	Conversion/%[b]	Yield/%[b]
1	**1b (A1)**	DIPEA	97	67
2	**4^Me b (A1)**	DIPEA	97	64
3	**6^H b (A1)**	DIPEA	96	64
4	**4^Me b (A2)**	DIPEA	98	54
5	**1b (A2)**	DIPEA	99	<15
6	**6^H b (A2)**	DIPEA	84	51
7[c]	**4^Me b (A3)**	TEA	97	79
8	**4^Me b (A1)**	TEA	91	64
9	**4^Me b (A1)**	TMEDA	52	32
10	**4^Me b (A1)**	DBU	96	72
11[d]	**4^Me b (A1)**	DIPEA	85	54
12[e]	**4^Me b (A1)**	DIPEA	62	28
13[f]	**4^Me b (A1)**	-	0	0
14[g]	**4^Me b (A1)**	DIPEA	0	0
15	Ru(bpy)$_3$Cl$_2$ **(A1)**	DIPEA	0	0
16	fac-Ir(ppy)$_3$ **(A1)**	DIPEA	27	16

[a] Procedure: Substrate 50 μmol, **PC** (2 mol%), amine (5 equiv.), HCOOH (2.5 equiv.) in 4 mL aqueous solution was degassed by nitrogen, and irradiated by blue light (12 W, λ_{max} = 462 nm) at ambient temperature for 10 h. [b] Determined by ^{1}H NMR spectroscopy by adding internal standard of 5,5'-dimethyl-2,2'-bipyridine. [c] Irradiated for 4 h. [d] Absence of HCOOH. [e] Presence of air (no degassing). [f] Absence of amine. [g] Absence of light.
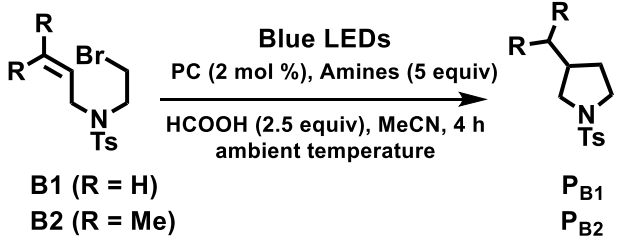
As the present bis-NHC Ir(III) complexes show strong absorption at λ > 400 nm, they were used to perform photo-

catalysis of the reductive cyclization of aryl bromides using blue LEDs. Among the bis-NHC Ir(III) complexes examined, **1b**, **4^Meb** and **6^Hb** displayed good photo-catalytic activity for the photo-catalytic reductive cyclization of aryl bromide (**A1**) in terms of both substrate conversion and product yield (Table 3).

In the case of another aryl bromide substrate **A2**, **4^Meb** showed both good substrate conversion and product yield (Table 4, entries 4 − 6). It was chosen as photo-sensitizer for optimization of the reaction conditions. A number of control experiments were performed, no reaction was observed in the absence of amine or light (entries 13 – 14). Lowering the loading of PC (Table 3, entry 4), the absence of HCOOH or exposure to air (entries 11 – 12) were observed to decrease the substrate conversion of this reaction. Interestingly, using 1,8-diazabicyclo[5.4.0]undec-7-ene (DBU, entry 10, $E_{onset}^{+/0} = 0.60$ V vs Cp$_2$Fe$^{+/0}$), also led to excellent substrate conversion and good product yield comparable to that obtained with tetramethylethylenediamine (TMEDA, entry 9, $E_{onset}^{+/0} = 0.11$ V vs Cp$_2$Fe$^{+/0}$, Fig.S9, ESI†). In contrast, the widely used photo-catalysts [Ru(bpy)$_3$]Cl$_2$ and *fac*-Ir(ppy)$_3$ (Table 4, entries 15 and 16) showed no or little conversion under similar conditions.

Table 5. Visible-light-induced C-C bond formation of alkyl bromide.

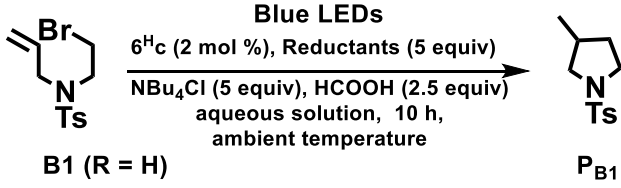| Entry[a]	PC	Amines	Conversion/%[b]	Yield/%[b]
1	Ru(bpy)$_3$Cl$_2$	DIPEA	19	5
2	*fac*-Ir(ppy)$_3$	DIPEA	90	72
3	**1b**	DIPEA	99	85
4	**4^Meb**	DIPEA	99	76
5	**6^Hb**	DIPEA	99	90
6	**4^Meb**	TEA	99	72
7	**4^Meb**	TMEDA	84	55
8	**4^Meb**	DBU	99	64
9	**4^Meb**	-	0	0
10[c]	**4^Meb**	DIPEA	27	15
11[d]	**4^Meb**	DIPEA	0	0
12[e]	**4^Meb**	DIPEA	0	0
13[f]	**4^Meb**	DIPEA	99	59.1

[a] Entry 1−11: R = H (substrate **A1**); Procedure: Substrate 50 μmol, PC (2 mol%), amine (5 equiv.) and HCOOH (2.5 equiv.) in 4 mL MeCN solution was degassed by nitrogen, and irradiated by blue light (12 W, λ_{max} = 462 nm) at 25 ºC. [b] Determined by ^{1}H NMR spectroscopy by adding internal standard of 5,5'-dimethyl-2,2'-bipyridine. [c] Absence of HCOOH (20 equiv.). [d] Absence of light. [e] Presence of TEMPO (radical trapping reagent, 2 equiv.) [f] Entry 13: R = Me (substrate **A2**).

The radical cyclization of the alkyl bromides, **B1** and **B2**, catalysed by **1b**, **4^Meb** or **6^Hb** proceed smoothly, with reasonable to excellent substrate conversion and product yields also. The

yield of cyclization of **B1** was improved to up to 90% (entry 5, Table 3) when formic acid was added and **6^Hb** was used as a photo-catalyst (PC). When 2,2,6,6-tetramethyl-1-piperidinyloxy (TEMPO) was added, the reaction was totally inhibited, indicating the involvement of radical intermediate in the reaction (entry 12).

The photo-catalytic reaction could be initiated from the oxidative quenching of **4^Meb*** with aryl/alkyl halide. This is because the excited state reduction potential of **4^Meb*** (E(Ir$^{IV/III*}$)$_{pc}$ = -1.51 V (*vs* SCE), Table S3, Fig. S9) can allow a direct one electron reduction of aryl/alkyl halide by **4^Meb***, leading to carbon-halogen (σ*(C-X)) bond cleavage to give alkyl radical in the case of sp^3 carbon or radical anion intermediate for sp^2 carbon.[86] Subsequent reactions of the alkyl radical or radical anion intermediate with C(sp^2)-H bond lead to C-C bond formation. An aminium radical cation generated from the oxidation of amine by [**4^Meb**]$^{+[83, 85]}$ could serve as an electron donor to complete the reductive process. In the case of [(ppy)$_2$Ir(dtbbpy)]PF$_6$,[83] its triplet excited state ([(ppy)$_2$Ir(dtbbpy)]$^{+*}$) reacts with DIPEA via a reductive quenching mechanism to generate Ir(II) species (E(Ir$^{III/II}$)$_{pc}$ = -1.51 V (*vs* SCE)[1], Fig. S9, ESI†), which initiates the subsequent reducing catalytic reaction.

Table 6. Visible-light-induced radical cyclization in aqueous solution.

Entry[a]	Solvents (H$_2$O/MeOH)[b]	Reductant	Conversion/%[c]	Yield/%[c]
1	3/1	Ascorbic Acid	23	10
2[d]	3/1	Ascorbic Acid	20	14
3	3/1	DIPEA	98	49
4[d,e]	3/1	DIPEA	90	21
5[d]	3/1	DIPEA	79	31
6	1/1	DIPEA	99	64
7	1/3	DIPEA	99	87
8	0/1	DIPEA	99	66

[a] Procedure: Substrate 50 μmol, **6^Hc** (2 mol%), reductant (5 equiv.), ^nBu$_4$NCl (5 equiv.) in 4 mL aqueous solution was degassed by nitrogen, and irradiated by blue light (12 W, λ_{max} = 462 nm) at 25 ºC. [b] Solvent system is used as water/methanol in volume ratio (v/v). [c] Determined by ^{1}H NMR spectroscopy by adding internal standard of 5,5'-dimethyl-2,2'-bipyridine. [d] Absence of HCOOH. [e] Absence of ^nBu$_4$NCl.

Interestingly, modifying N-substituent of bis-NHC ligand from alkyl group to glucose moiety renders photo-catalyst **6^Hc** soluble in aqueous media. At outset, we examined the **6^Hc**-catalysed reductive cyclization of **B1** in a mixture of H$_2$O/MeOH (3:1) with ascorbic acid as reductant, but both the substrate conversion and product yield were low. The use of diisopropylethylamine (DIPEA) as reductant instead of ascorbic acid and addition of tetrabutylammonium chloride improved the

Page 9 of 14

Chemical Science

View Article Online
DOI: 10.1039/C5SC04458H

Chemical Science

ARTICLE

conversion and yield to 98% and 49%, respectively. Increasing vol% of methanol in aqueous solution to 75% leads to 99% conversion and 87% product yield. To the best of our knowledge, this is the first example of visible-light-driven radical cyclization for synthesis of pyrrolidine in aqueous media.

Visible-light-driven CO_2 reduction

There is a surge of interest to develop photo-catalytic CO_2 reduction using earth abundant metal complexes as catalyst and luminescent cyclometalated Ir(III) complexes particularly *fac*-Ir(ppy)$_3$ as PC. Nevertheless, several recent reports drawn out the attention of the instability of *fac*-Ir(ppy)$_3$, which is a challenge for achieving efficient light-driven CO_2 reduction in a long run.[55, 57, 63] In view of the good photo-stability of $4^{Me}b$, we have been prompted to investigate the visible-light-driven CO_2 reduction by utilizing $4^{Me}b$ in combination with the recent reported [Co(TPA)Cl]Cl complex.[57]

A CO_2-saturated MeCN/triethylamine solution (4/1, v:v; 4 mL) containing catalytic amount of $4^{Me}b$ and [Co(TPA)Cl]Cl was irradiated by blue LEDs (12 w) for a specified time period, and the evolved gases were separated and identified by a GC-TCD equipped with a molecular sieve column. The volume of H_2 and CO gases were calculated by using CH_4 as the internal standard.

As shown in Fig. 7a and Fig. 7b, the amount of CO and H_2 generated from the reaction mixture is found to show strong dependence on the concentrations of $4^{Me}b$ and Co(II) catalysts. Particularly, the highest TON value of over 5000 can be accomplished at 0.5 μM of Co(II), while no generation of gases is found at low concentration of Co(II) (50 nM; Fig. S11, ESI†). Similarly, only negligible amount of product gases can be detected after irradiation for 24 h when [Ir] (0.005 mM) is lower than [Co] (0.05 mM). With the representative system containing $4^{Me}b$ (0.5 mM) and Co(II) (0.005 mM), (Fig. 7c) the visible-light-driven CO_2 reduction in three parallel reaction runs gives TON (CO) > 2400 (conversion of about 18 mL of CO_2 into 1 mL of CO) with excellent selectively in generating CO over H_2 in gaseous phase (>95%) after reaction for 72 h. This result is better than that of the system utilizing *fac*-Ir(ppy)$_3$ as PC, which reveals only TON (CO) > 900 and selectivity (CO) of 85% under similar reaction conditions.[57]

In order to confirm the roles of catalysts in photo-driven CO_2 reduction, several control experiments were performed (Table S5, ESI†). Firstly, in the absence of Co(II) complex, no CO gas was observed in a CO_2-saturated MeCN/TEA (4:1, V:V; 4 mL) solution after irradiation for 24 h. On the other hand, in the absence of light, sacrificial amine or PC, the reaction mixture only gives negligible amount of CO. To ascertain the catalytic role of Co(II) complex in the reaction, mercury was added to the reaction mixture in order to exclude the possibility of CO generation from heterogeneous Co nanoparticles. To specify, 29.2 μmol of CO (0.714 mL, TON 146) could be generated from the solution with [Ir] (0.5 mM), [Co] (0.05 mM) and elementary Hg (1 mL) after irradiation for 18h, and this result is comparable with that using the solution mixture without Hg (28.4 μmol of CO formed, TON 142).
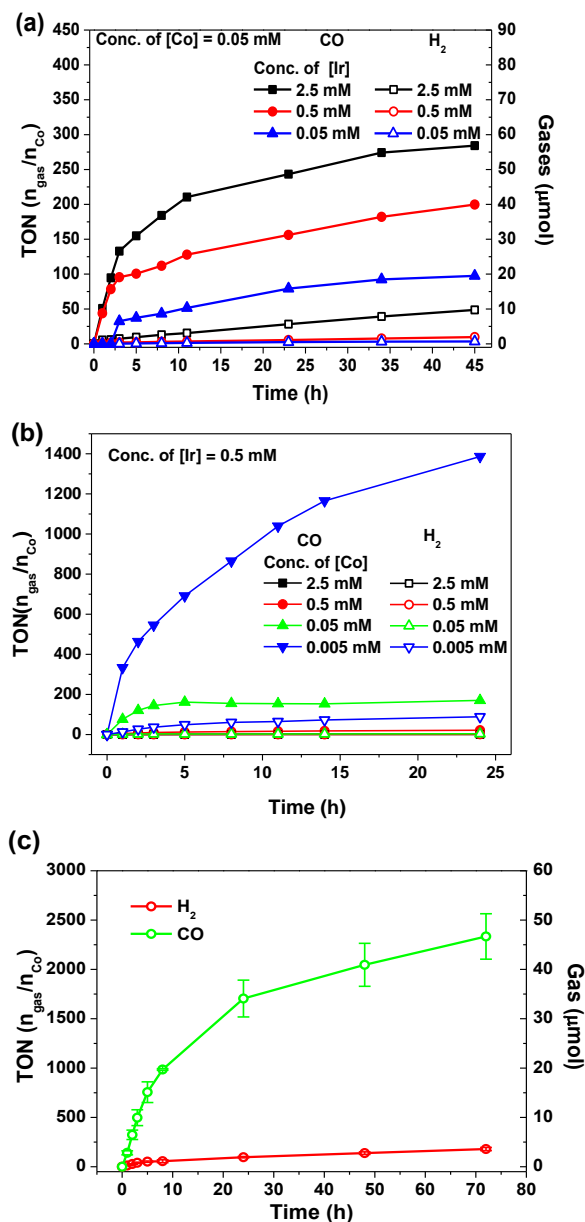

Fig. 7 TON value and amounts of gases (CO and H_2) generation from CO_2 in a CO_2-saturated MeCN/TEA (4/1, v/v, 4 mL in total) solution as a function of irradiation time: concentration dependence of a) PC $4^{Me}b$ and b) catalyst **[Co(TPA)Cl]Cl**; c) a solution containing 0.005 mM **[Co(TPA)Cl]Cl**, 0.5 mM $4^{Me}b$ was irradiated using blue LEDs (12 w) based on the averaged results from three parallel reaction runs.

Cellular imaging and cell viability assay

We have a long-standing interest on luminescent transition metal complexes particularly those supported by NHC ligands that display anti-cancer activities.[9, 16, 87-90] The luminescence would allow direct monitoring of cellular uptake and tracking of cellular location in cancer cells by fluorescence microscopy, and such properties of transition metal NHC complexes have been demonstrated to be useful in elucidation of anti-cancer mechanism of action. In this work, in view of their favourable photophysical properties, the *in vitro* cytotoxicity of the bis-

ARTICLE

NHC Ir(III) complexes against HeLa cells was investigated by MTT assay. As shown in Table S6 (ESI†), the Ir(III) complexes display potent cytotoxicity, with IC_{50} values ranging from 0.5 to 56.1 μM depending on the lipophilicity and structures of the Ir(III) complexes. Those complexes with butyl groups on the bis-NHC ligand are more cytotoxic than those having NHC ligands with glucose unit.

Since complexes **1b**, **4^Meb**, **6^Ha**, **6^Hb** and **6^Hc** demonstrate outstanding photophysical properties i.e. high quantum yield with long-lived electronic excited state, cellular imaging of the entitled complexes in HeLa cells were performed. After treatment of human cervical cancer cells (HeLa) with the Ir(III) complexes for 15 min, strong green/yellow luminescence were observed in cytoplasm (but not nucleus) of cancer cells, as revealed by fluorescence microscopy (Fig. 8). Co-localization analyses indicate that the emission of these complexes are mainly localized in endoplasmic reticulum (ER), which is stained by red-emissive ER-specific ER-Tracker^EM; high Pearson's correlation coefficient (R) between the emissions of complexes and ER-Tracker^EM is found (for example, **6^Hb** shows a high R value of 0.80). Consistently, these complexes do not accumulate in other organelles such as lysosome or mitochondria, as shown by the poor co-localization of the emissions of the complexes with the emission of Lyso-Tracker® and Mito-Tracker® respectively (Fig. S13, ESI†). Noticeably, **1b**+ (both the counter anions of triflate and chloride) in our laboratory, were found to be specifically localized in ER of cancer cells (Fig.S14), but not as reported into mitochondria[73]. With the consideration of specific accumulation of the complexes in ER, the cytotoxic properties of the complexes may originate from the induction of ER stress[88] and immunogenic cell death.[91]
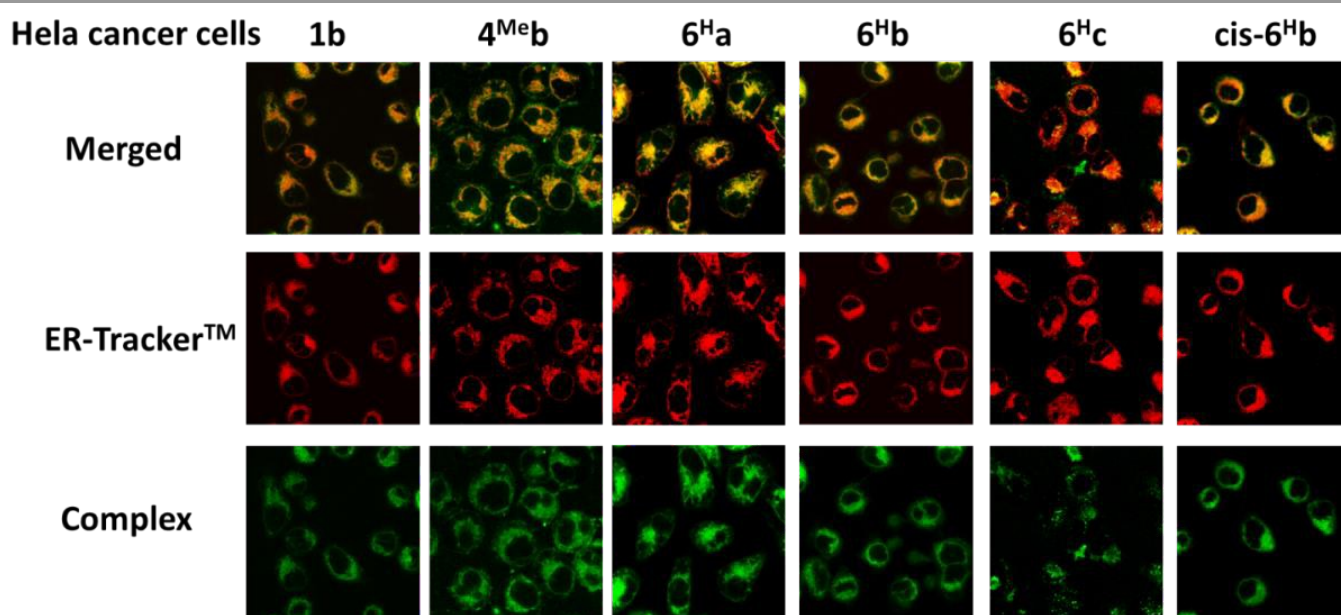

Fig. 8 Fluorescence microscopy images of HeLa cancer cells incubated with the Ir(III) NHC complexes: merged (top), ER-tracker^EM (middle) and complexes (bottom). Complexes were excited at 340 nm using an emission filter of 510 nm. ER-tracker^EM was excited at 546 nm using an emission filter of >580 nm.

Discussion

Herein, this work reveals the potential impact and usefulness of bis-NHC ligands for the development of robust metal photo-catalysts. Compared with the well-known complexes *fac*-Ir(ppy)₃, this series of bis-NHC Ir(III) complexes exhibits: i) outstanding photo-stability under visible light irradiation; ii) good photo-catalytic performance for several photo-electrochemically reactions; and iii) long-lived emissive excited states.

Stability of NHC metal complexes

The most important feature of metal-ligand bonding between transition metals and NHCs, can be rationalized as the σ-coordination (sp^2-hybridized lone pair electron) from NHCs. The contribution of both π-back-bonding into carbene *p*-orbital and π-donation from the carbene *p*-orbital might be considered as less significant for NHC metal complexes. These behaviours are similar to the coordination characteristics of phosphines, but NHCs are in general better electron-donors than phosphines. Thus, the stronger metal–ligand interaction renders NHC–metal coordination less labile than metal–phosphine bonding and the NHC complexes are more thermally and oxidatively stable.[92] The distinct electronic properties and coordination chemistry of NHCs can also lead to improved catalytic activity of the metal complexes, owing to the increased catalyst stability and consequently lower rates of catalyst decomposition.[68] In previous section, the studies on the photo-stability of **4^Meb** and *fac*-Ir(ppy)₃ have revealed the outstanding stabilization contribution from bis-NHC carbene ligands. Thus this might be one reason that explains the better performance for photo-catalytic reactions using the present bis-NHC Ir(III) complexes as PC.

Role of bis-NHC ligands in tuning emission energy and lifetimes

A comparison between the photophysical data of bis-NHC Ir(III) complexes with two notable Ir(III) complexes (*fac*-Ir(ppy)$_3$ and (ppy)$_2$Ir(acac) (**1d**)) will be helpful in understanding the role of NHC on the strong absorptivities, high emission efficiencies and long lifetimes properties of the present bis-NHC Ir(III) complexes. On the basis of DFT calculations on **1a** as the representative example (Fig. S4, ESI†), the lowest-energy absorption bands of **1a**, **1d** and *fac*-Ir(ppy)$_3$ are ascribed to the HOMO→LUMO transitions, and the energy of which is sensitive to the charge of ancillary ligands. The transition energy of *fac*-Ir(ppy)$_3$ and **1d** with the negatively charge ancillary ligands (C^N and acac) are quite close with wavelength of 416 and 414 nm respectively. However, for **1a** with the neutral ancillary ligand (bis-NHC), the HOMO→LUMO transition is markedly hypsochromically shifted to 369 nm, which is consistent with the experimental observations. Fig. S10 (ESI†) shows the surfaces and the energies of HOMO and LUMO of **1a**, *fac*-Ir(ppy)$_3$ and **1d**. On the whole, HOMO contains comparable components of iridium and C^N ligand, and LUMO is mainly localized on the C^N ligand. Thus, the transition can be assigned as admixtures of metal-to-ligand charge transfer (MLCT) and ligand centered (LC) π–π* transition, which is in accordance with the assignments reported in literatures.

The different amounts of metal participations into the frontier molecular orbitals of **1a**, **1d** and Ir(ppy)$_3$, as deduced by TD-DFT calculations, can account for the photophysical properties and long emission lifetimes of the Ir(III) NHC complexes. As shown in Fig. S10 (ESI†), *fac*-Ir(ppy)$_3$ and **1d** have similar energy levels in HOMO and LUMO (around -4.5 eV and -2.0 eV). By simply substitution of the negatively charge ancillary ligands (C^N and acac) in Ir(ppy)$_3$ and **1d** by neutral NHC ligand, **1a** is found to show lower energy levels of HOMO and LUMO (about -5.2 eV and -2.4 eV). This can be explained by the less electron-donating effect of the neutral NHC ligand than that of the negatively charged auxiliary ligands, as well as certain contribution of the stabilization of dπ(Ir) by the π-acceptor orbitals of NHC ligand of **1a**.[68] As a result, the energy level of HOMO of **1a** is 700 mV lower that of **1d**, which coincides with the experimental observation that the oxidation potential of **1a** is 410 mV more positive than that of **1d**. On the other hand, the transition energy of HOMO→LUMO in **1a** is estimated to be 0.3 eV larger than that in Ir(ppy)$_3$ and **1d**, which may account for the blue shift of low-energy absorption of **1a** (369 nm vs 410 nm), as compared to that of **1d** and Ir(ppy)$_3$, in UV-vis absorption spectra. Notably, TD-DFT calculation reveals that frontier molecular orbitals of **1a** shows a smaller metal character than those of **1d** (Ir character in HOMO of **1a** and **1d** are found to be ~30 and ~40% respectively), and hence the triplet excited states of **1a** are likely to have smaller metal character. This would probably slow down the spin-orbit coupling, resulting in slower radiative and non-radiative T$_1$→S$_0$ decay for **1a**. As a result, **1a** shows a longer emission lifetime than that of **1d**.

Triplet excited states for photo-catalytic reactivity

In addition to the photo-stability and strong absorptivity in visible light region, the long-lived triplet excited states especially its propensity to loss an electron, to a large extent, are believed to be crucial for the photo-catalytic properties of the complexes. The long triplet excited state lifetime of **4^{Me}b** is beneficial for bi-molecular photochemical reactions allowing the electron-transfer pathways to have sufficient time to take place prior to the decay of the excited state to the ground state.

Considering the fact that the excited-state of [Ru(bpy)$_3$]$^{2+}$ (E(Ru$^{II*/I}$) = 0.77 V vs SCE) is a more powerful oxidative potential than that of **4^{Me}b** (E(Ir$^{III*/II}$) = 0.51 V vs SCE, Table S3) and no radical cyclization products is obtained when using [Ru(bpy)$_3$]$^{2+}$, the photo-catalytic route via reductive quenching cycle is not feasible. The photo-catalytic reaction would possibly be initialized via oxidative quenching cycle of excited state of photo-catalyst. By carefully examining transient-absorption spectra of triplet state of **4^{Me}b** in MeCN, newly generated long-lived species by using higher energy laser beams were observed (Fig.S8b-S8g). This long-lived species was found to be increased in the presence of substrate **A1**, and could be quenched by DIPEA. This long-lived species might be Ir(IV), which is generated by single electron transfer from [**4^{Me}b**]* to **A1**. The calculated excited-state reduction potential of **4^{Me}b** (E(Ir$^{IV/III*}$) = -1.51 V vs SCE, Table S3) reveals that **4^{Me}b** is not a stronger photo-reductant than *fac*-Ir(ppy)$_3$ (E(Ir$^{IV/III*}$) = -1.73 V vs SCE).[37, 93] However, performance of **4^{Me}b** in visible-light-driven radical cyclization and CO$_2$ reduction prove to be better than that of *fac*-Ir(ppy)$_3$. For example, the conversion of substrates **A1**/**B1** to indoline/pyrrolidine by **4^{Me}b** (97%/99%) are higher than that by *fac*-Ir(ppy)$_3$ (27%/90%). Therefore, there should be other reasons to account for the good performance of **4^{Me}b** in photo-catalysis. Plausible reasons could be: i) the generated Ir(IV) [**4^{Me}b**]$^+$ (E(Ir$^{IV/III}$) = 0.96 V vs SCE, Table S3) are more easily reduced by amines than [*fac*-Ir(ppy)$_3$]$^+$ (E(Ir$^{IV/III}$) = 0.77 V vs SCE); and ii) the higher photo-stability of **4^{Me}b** compared with that of *fac*-Ir(ppy)$_3$.

Consequently, the excellent photo-stability, strong absorptivity, long-lived lifetimes and the photo-ionization behaviours of our bis-NHC Ir(III) complexes possibly make the photolysis of long-lived excited state of Ir(III)* more easily to Ir(IV) and thus promote the radical cyclization to proceed in a catalytic cycle.

Diversities of biological activities of Ir(III) complexes with different *N*-substituents on NHC ligands

Although *N*-substituents of NHC ligands are found to show negligible effects on the luminescent properties of the bis-NHC Ir(III) complexes, they have a determinant role on the physical properties and hence the anti-cancer activities of the complexes. For example, complexes with *N*-butyl substituents on the bis-NHC ligands generally display lower IC$_{50}$ values than those with *N*-methyl substituents (Table S6 in ESI†). This is probably attributed to the increase in lipophilicity of the complexes, resulting in better permeability through cellular membrane and higher accumulation of the complexes in cancer cells. The fast cellular uptake of the complexes is supported by the strong

luminescence observed in HeLa cells after incubation of the cells with the complexes for 15 min (Fig. 8 and S12 in ESI†). On the other hand, the glucose-functionalized NHC ligands render the complexes good aqueous solubility and more hydrophilic in nature, leading to likely slower cellular uptake as well as the reduced cytotoxicity toward cancer cells. It is noteworthy that the complexes accumulate in cellular ER as revealed by fluorescence microscopy images of the co-staining experiments. This can consequently induce ER stress[88] and immunogenic cell death, which probably account for the high cytotoxicity of the complexes. Further manipulations of the functionalities on NHC ligands of the Ir(III) complexes may realize the development of a new class of diagnostic and/or therapeutic agents.

Conclusions

A new series of cyclometalated Ir(III) complexes bearing bis-NHC ligand has been demonstrated as strongly luminescent materials and promising photo-catalysts for visible-light-driven radical cyclization and CO_2 reduction and biological theranostic agents. Owing to the high stability of Ir−C^{NHC} bond, these bis-NHC Ir(III) complexes show excellent photo-stability compared with widely-used PC, such as *fac*-Ir(ppy)$_3$ and [Ru(bpy)$_3$]$^{2+}$. With long-lived triplet excited states and rich photoredox properties, **4^{Me}c** can undergo photo-ionization in aqueous media as supported by transient absorption experiments, while **4^{Me}b** is found to be a more effective catalyst for radical cyclization and CO_2 reduction than *fac*-Ir(ppy)$_3$ under visible-light irradiation. Interestingly, water-soluble **6^{H}c**, which contains glucose moiety on the bis-NHC ligands, has been demonstrated as the first PC for the synthesis of pyrrolidine in aqueous media. In addition, through modulations of the chemical structures of the cyclometalated ligands and/or *N*-substituents on the bis-NHC ligands, the Ir(III) complexes have been found to show different luminescent properties as well as anti-cancer activities, indicating the potential of the complexes as theranostic agents.

Acknowledgements

Notes and references

ᵃ State Key Laboratory of Synthetic Chemistry, Institute of Molecular Functional Materials, HKU-CAS Joint Laboratory on New Materials and Department of Chemistry, The University of Hong Kong, Pokfulam Road, Hong Kong, China

ᵇ HKU Shenzhen Institute of Research and Innovation, Shenzhen, China

ᶜ Department of Applied Biology and Chemical Technology, The Hong Kong Polytechnic University, Hung Hom, Hong Kong.
E-mails: sharonlf.chan@polyu.edu.hk; cmche@hku.hk

1. M. S. Lowry, J. I. Goldsmith, J. D. Slinker, R. Rohl, J. Robert A. Pascal, G. G. Malliaras and S. Bernhard, *Chem. Mater.*, 2005, **17**, 5712-5719.
2. C. Yang, S.-L. Lai, S. L.-F. Chan, K.-H. Low, G. Cheng, K.-T. Yeung, C.-C. Kwok and C.-M. Che, *Chem. Asian J.*, 2014, **9**, 3572-3585.
3. A. B. Tamayo, B. D. Alleyne, P. I. Djurovich, S. Lamansky, I. Tsyba, N. N. Ho, R. Bau and M. E. Thompson, *J. Am. Chem. Soc.*, 2003, **125**, 7377-7387.
4. M. A. Baldo, D. F. O'Brien, Y. You, A. Shoustikov, S. Sibley, M. E. Thompson and S. R. Forrest, *Nature*, 1998, **395**, 151-154.
5. M. A. Baldo, M. E. Thompson and S. R. Forrest, *Nature*, 2000, **403**, 750-753.
6. S. C. F. Kui, P. K. Chow, G. Cheng, C.-C. Kwok, C. L. Kwong, K.-H. Low and C.-M. Che, *Chem. Commun.*, 2013, **49**, 1497-1499.
7. K. Li, G. Cheng, C. Ma, X. Guan, W.-M. Kwok, Y. Chen, W. Lu and C.-M. Che, *Chem. Sci.*, 2013, **4**, 2630-2644.
8. S. C. F. Kui, P. K. Chow, G. S. M. Tong, S.-L. Lai, G. Cheng, C.-C. Kwok, K.-H. Low, M. Y. Ko and C.-M. Che, *Chem. Eur. J.*, 2013, **19**, 69-73.
9. K. Li, T. Zou, Y. Chen, X. Guan and C. M. Che, *Chem. Eur. J.*, 2015, **21**, 7441-7453.
10. E. S.-H. Lam, D. P.-K. Tsang, W. H. Lam, A. Y.-Y. Tam, M.-Y. Chan, W.-T. Wong and V. W.-W. Yam, *Chem. Eur. J.*, 2013, **19**, 6385-6397.
11. Z. He, W.-Y. Wong, X. Yu, H.-S. Kwok and Z. Lin, *Inorg. Chem.*, 2006, **45**, 10922-10937.
12. S.-L. Lai, L. Wang, C. Yang, M.-Y. Chan, X. Guan, C.-C. Kwok and C.-M. Che, *Adv. Func. Mater.*, 2014, **24**, 4655-4665.
13. W. X. Ni, M. Li, J. Zheng, S. Z. Zhan, Y. M. Qiu, S. W. Ng and D. Li, *Angew. Chem. Int. Ed.*, 2013, **52**, 13472-13476.
14. M.-C. Tang, D. P.-K. Tsang, M. M.-Y. Chan, K. M.-C. Wong and V. W.-W. Yam, *Angew. Chem. Int. Ed.*, 2013, **52**, 446-449.
15. W.-P. To, K. T. Chan, G. S. M. Tong, C. Ma, W.-M. Kwok, X. Guan, K.-H. Low and C.-M. Che, *Angew. Chem. Int. Ed.*, 2013, **52**, 6648-6652.
16. T. Zou, C. T. Lum, S. S.-Y. Chui and C.-M. Che, *Angew. Chem. Int. Ed.*, 2013, **52**, 2930-2933.
17. F.-F. Hung, W.-P. To, J.-J. Zhang, C. Ma, W.-Y. Wong and C.-M. Che, *Chem. Eur. J.*, 2014, **20**, 8604-8614.
18. X.-S. Xiao, W.-L. Kwong, X. Guan, C. Yang, W. Lu and C.-M. Che, *Chem. Eur. J.*, 2013, **19**, 9457-9462.
19. R. Visbal, J. M. Lopez-de-Luzuriaga, A. Laguna and M. C. Gimeno, *Dalton Trans.*, 2014, **43**, 328-334.
20. C.-M. Che, C.-C. Kwok, S. C. F. Kui, S.-L. Lai and K.-H. Low, in *Compr. Inorg. Chem. II (2ⁿᵈ ed.)*, ed. J. R. Poeppelmeier, Elsevier, Amsterdam, 2013, pp. 607-655.
21. H. Yersin and W. J. Finkenzeller, in *Highly Efficient OLEDs with Phosphorescent Materials*, Wiley-VCH Verlag GmbH & Co. KGaA, 2008, pp. 1-97.
22. Y. Ma, H. Zhang, J. Shen and C. Che, *Synth. Met.*, 1998, **94**, 245-248.

Page 13 of 14

Chemical Science

View Article Online
DOI: 10.1039/C5SC04458H

Chemical Science

ARTICLE

Chemical Science Accepted Manuscript

23. K. K.-W. Lo, A. W.-T. Choi and W. H.-T. Law, *Dalton Trans.*, 2012, **41**, 6021-6047.

24. F. L. Thorp-Greenwood, R. G. Balasingham and M. P. Coogan, *J. Organomet. Chem.*, 2012, **714**, 12-21.

25. J. N. Demas and B. A. DeGraff, *Anal. Chem.*, 1991, **63**, 829A-837A.

26. V. W.-W. Yam and K. M.-C. Wong, *Chem. Commun.*, 2011, **47**, 11579-11592.

27. T. P. Yoon, M. A. Ischay and J. Du, *Nat. Chem.*, 2010, **2**, 527-532.

28. S. Lamansky, P. Djurovich, D. Murphy, F. Abdel-Razzaq, R. Kwong, I. Tsyba, M. Bortz, B. Mui, R. Bau and M. E. Thompson, *Inorg. Chem.*, 2001, **40**, 1704-1711.

29. J. Li, P. I. Djurovich, B. D. Alleyne, M. Yousufuddin, N. N. Ho, C. J. Thomas, J. C. Peters, R. Bau and M. E. Thompson, *Inorg. Chem.*, 2005, **44**, 1713-1727.

30. A. F. Rausch, M. E. Thompson and H. Yersin, .*J. Phys. Chem. A*, 2009, **113**, 5927-5932.

31. S. Lamansky, P. Djurovich, D. Murphy, F. Abdel-Razzaq, H.-E. Lee, C. Adachi, P. E. Burrows, S. R. Forrest and M. E. Thompson, *J. Am. Chem. Soc.*, 2001, **123**, 4304-4312.

32. K. K.-W. Lo, B. T.-N. Chan, H.-W. Liu, K. Y. Zhang, S. P.-Y. Li and T. S.-M. Tang, *Chem. Commun.*, 2013, **49**, 4271-4273.

33. S. P.-Y. Li, T. S.-M. Tang, K. S.-M. Yiu and K. K.-W. Lo, *Chem. Eur. J.*, 2012, **18**, 13342-13354.

34. W. H.-T. Law, L. C.-C. Lee, M.-W. Louie, H.-W. Liu, T. W.-H. Ang and K. K.-W. Lo, *Inorg. Chem.*, 2013, **52**, 13029-13041.

35. K. K.-W. Lo and K. K.-S. Tso, *Inorg. Chem. Front.*, 2015,**2**, 510-524.

36. K. K.-W. Lo and K. Y. Zhang, *RSC Adv.*, 2012, **2**, 12069-12083.

37. C. K. Prier, D. A. Rankic and D. W. C. MacMillan, *Chem. Rev.*, 2013, **113**, 5322-5363.

38. D. A. Nicewicz and D. W. C. MacMillan, *Science*, 2008, **322**, 77-80.

39. Z. Lu and T. P. Yoon, *Angew. Chem. Int. Ed.*, 2015, **51**, 10329-10332.

40. M. A. Ischay, M. E. Anzovino, J. Du and T. P. Yoon, *J. Am. Chem. Soc.*, 2008, **130**, 12886-12887.

41. D. M. Schultz and T. P. Yoon, *Science*, 2014, **343**, 1239176.

42. J. W. Tucker, J. D. Nguyen, J. M. R. Narayanam, S. W. Krabbe and C. R. J. Stephenson, *Chem. Commun.*, 2010, **46**, 4985-4987.

43. J. M. R. Narayanam and C. R. J. Stephenson, *Chem. Soc. Rev.*, 2011, **40**, 102-113.

44. J. M. R. Narayanam, J. W. Tucker and C. R. J. Stephenson, *J. Am. Chem. Soc.*, 2009, **131**, 8756-8757.

45. J. D. Nguyen, E. M. D'Amato, J. M. R. Narayanam and C. R. J. Stephenson, *Nat. Chem.*, 2012, **4**, 854-859.

46. P.-K. Chow, G. Cheng, G. S. M. Tong, W.-P. To, W.-L. Kwong, K.-H. Low, C.-C. Kwok, C. Ma and C.-M. Che, *Angew. Chem. Int. Ed.*, 2015, **54**, 2084-2089.

47. J.-J. Zhong, Q.-Y. Meng, G.-X. Wang, Q. Liu, B. Chen, K. Feng, C.-H. Tung and L.-Z. Wu, *Chem. Eur. J.*, 2013, **19**, 6443-6450.

48. B. Kumar, M. Llorente, J. Froehlich, T. Dang, A. Sathrum and C. P. Kubiak, *Annu. Rev. Phys. Chem.*, 2012, **63**, 541-569.

49. C. D. Windle and R. N. Perutz, *Coord. Chem. Rev.*, 2012, **256**, 2562-2570.

50. C. Costentin, M. Robert and J.-M. Savéant, *Chem. Soc. Rev.*, 2012, **42**, 2423-2436.

51. D. Behar, a. T. Dhanasekaran, P. Neta, C. M. Hosten, a. D. Ejeh, P. Hambright and E. Fujita, *J. Phys. Chem. A*, 1998, **102**, 2870-2877.

52. R. Ziessel, J. Hawecker and J.-M. Lehn, *Helv. Chim. Acta.*, 1986, **69**, 1065-1084.

53. H. Hori, F. P. A. Johnson, K. Koike, O. Ishitani and T. Ibusuki, *J. Photochem. Photobio. A: Chem.*, 1996, **96**, 171-174.

54. S. Sato, T. Morikawa, T. Kajino and O. Ishitani, *Angew. Chem. Int. Ed.*, 2013, **52**, 988-992.

55. V. S. Thoi, N. Kornienko, C. G. Margarit, P. Yang and C. J. Chang, *J. Am. Chem. Soc.*, 2013, **135**, 14413-14424.

56. J. Bonin, M. Robert and M. Routier, *J. Am. Chem. Soc.*, 2014, **136**, 16768-16771.

57. S. L.-F. Chan, T. L. Lam, C. Yang, S.-C. Yan and N. M. Cheng, *Chem. Commun.*, 2015, **51**, 7799-7801.

58. L. Chen, Z. Guo, X.-G. Wei, C. Gallenkamp, J. Bonin, E. Anxolabéhère-Mallart, K.-C. Lau, T.-C. Lau and M. Robert, *J. Am. Chem. Soc.*, 2015, **137**, 10918-10921.

59. R. S. Khnayzer, V. S. Thoi, M. Nippe, A. E. King, J. W. Jurss, K. A. El Roz, J. R. Long, C. J. Chang and F. N. Castellano, *Energy & Environ. Sci.*, 2014, **7**, 1477-1488.

60. C.-F. Leung, S.-M. Ng, C.-C. Ko, W.-L. Man, J. Wu, L. Chen and T.-C. Lau, *Energy & Environ. Sci.*, 2012, **5**, 7903-7907.

61. A. B. Tossi and H. Görner, *J. Photochem. and Photobio. B: Bio.* 1993, **17**, 115-125.

62. Y.-J. Yuan, Z.-T. Yu, X.-J. Liu, J.-G. Cai, Z.-J. Guan and Z.-G. Zou, *Sci. Rep.*, 2014, **4**, 4045.

63. S. Schmidbauer, A. Hohenleutner and B. König, *Beilstein J. Org. Chem.*, 2013, **9**, 2088-2096.

64. W. A. Herrmann, *Angew. Chem. Int. Ed.*, 2002, **41**, 1290-1309.

65. A. Azua, S. Sanz and E. Peris, *Chem. Eur. J.*, 2015, **17**, 3963-3967.

66. Y. Unger, A. Zeller, M. A. Taige and T. Strassner, *Dalton Trans.*, 2009, 4786-4794.

67. A. G. Tennyson, E. L. Rosen, M. S. Collins, V. M. Lynch and C. W. Bielawski, *Inorg. Chem.*, 2009, **48**, 6924-6933.

68. M. N. Hopkinson, C. Richter, M. Schedler and F. Glorius, *Nature*, 2014, **510**, 485-496.

69. D. Martin, M. Melaimi, M. Soleilhavoup and G. Bertrand, *Organometallics*, 2011, **30**, 5304-5313.

70. B. Rao, H. Tang, X. Zeng, L. Liu, M. Melaimi and G. Bertrand, *Angew. Chem. Int. Ed.*, 2015, **54**, 14915-14919.

71. L.-A. Schaper, S. J. Hock, W. A. Herrmann and F. E. Kühn, *Angew. Chem. Int. Ed.*, 2013, **52**, 270-289.

72. C.-H. Yang, J. Beltran, V. Lemaur, J. Cornil, D. Hartmann, W. Sarfert, R. Fröhlich, C. Bizzarri and L. De Cola, *Inorg. Chem.*, 2010, **49**, 9891-9901.

73. Y. Li, C.-P. Tan, W. Zhang, L. He, L.-N. Ji and Z.-W. Mao, *Biomater.*, 2015, **39**, 95-104.

74. J. Jin, H.-W. Shin, J. H. Park, J. H. Park, E. Kim, T. K. Ahn, D. H. Ryu and S. U. Son, *Organometallics*, 2013, **32**, 3954-3959.

75. D. N. Kozhevnikov, V. N. Kozhevnikov, M. Z. Shafikov, A. M. Prokhorov, D. W. Bruce and J. A. Gareth Williams, *Inorg. Chem.*, 2011, **50**, 3804-3815.

76. E. J. Hart and J. W. Boag, *J. Am. Chem. Soc.*, 1962, **84**, 4090-4095.

77. M. H. Elkins, H. L. Williams, A. T. Shreve and D. M. Neumark, *Science*, 2013, **342**, 1496-1499.

78. K. C. Cho and C. M. Che, *Chem. Phys. Lett.*, 1986, **124**, 313-315.

79. R. Y. N. Gengler, D. S. Badali, D. Zhang, K. Dimos, K. Spyrou, D. Gournis and R. J. D. Miller, *Nat. Commun.*, 2013, **4**, 2560.

Chemical Science

View Article Online

DOI: 10.1039/C5SC04458H

Page 14 of 14

Chemical Science

ARTICLE

80. A. K. El Omar, U. Schmidhammer, P. Pernot, S. Murata and M. Mostafavi, *J. Phys. Chem. A*, 2012, **116**, 11989-11996.

81. C. Xia, J. Peon and B. Kohler, *J. Chem. Phys.*, 2002, **117**, 8855-8866.

82. A. Juris, V. Balzani, P. Belser and A. von Zelewsky, *Helv. Chim. Acta*, 1981, **64**, 2175-2182.

83. H. Kim and C. Lee, *Angew. Chem. Int. Ed.*, 2012, **51**, 12303-12306.

84. M. Majek, U. Faltermeier, B. Dick, R. Pérez-Ruiz and A. Jacobi von Wangelin, *Chem. Eur. J.*, 2015, **21**, 15496-15501.

85. G. Revol, T. McCallum, M. Morin, F. Gagosz and L. Barriault, *Angew. Chem. Int. Ed.*, 2013, **52**, 13342-13345.

86. M. Arun Prasad and M. V. Sangaranarayanan, Chem. Phys. Lett., 2005, **414**, 55-60.

87. R. W.-Y. Sun, A. L.-F. Chow, X.-H. Li, J. J. Yan, S. S.-Y. Chui and C.-M. Che, *Chem. Sci.*, 2011, **2**, 728-736.

88. T. Zou, C.-N. Lok, Y. M. E. Fung and C.-M. Che, *Chem. Commun.*, 2013, **49**, 5423-5425.

89. T. Zou, C. T. Lum, C.-N. Lok, W.-P. To, K.-H. Low and C.-M. Che, *Angew. Chem. Int. Ed.*, 2014, **53**, 5810-5814.

90. J. L.-L. Tsai, A. O.-Y. Chan and C.-M. Che, *Chem. Commun.*, 2015, **51**, 8547-8550.

91. D. Y. Q. Wong, W. W. F. Ong and W. H. Ang, *Angew. Chem. Int. Ed.*, 2015, **54**, 6483-6487.

92. C. M. Crudden and D. P. Allen, *Coord. Chem. Rev.*, 2004, **248**, 2247-2273.

93. L. Flamigni, A. Barbieri, C. Sabatini, B. Ventura and F. Barigelletti, *Top. Curr. Chem.* eds. V. Balzani and S. Campagna, Springer Berlin / Heidelberg, 2007, vol. 281, pp. 143-203.

Chemical Science Accepted Manuscript